J. Appl. Comput. Mech., 4(5) (2018) 402-419
DOI: 10.22055/JACM.2018.24672.1205
ISSN: 2383-4536
jacm.scu.ac.ir

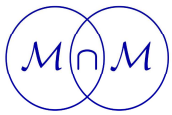

Journal of
Applied and Computational Mechanics

Research Paper

On the Geometrically Nonlinear Analysis of Composite Axisymmetric Shells

M. Rezaiee-Pajand[1], E. Arabi[2]

[1] Department of Civil Engineering, Ferdowsi University of Mashhad, Mashhad, 9177948974, Iran, rezaiee@um.ac.ir
[2] Department of Civil Engineering, Ferdowsi University of Mashhad, Mashhad, 9177948974, Iran, elias.arabi@mail.um.ac.ir

Received January 09 2018; Revised February 19 2018; Accepted for publication February 27 2018.
Corresponding author: M. Rezaiee-Pajand, rezaiee@um.ac.ir

Abstract. Composite axisymmetric shells have numerous applications; many researchers have taken advantage of the general shell element or the semi-analytical formulation to analyze these structures. The present study is devoted to the nonlinear analysis of composite axisymmetric shells by using a 1D three nodded axisymmetric shell element. Both low and higher-order shear deformations are included in the formulation. The displacement field is considered to be nonlinear function of the nodal rotations. This assumption eliminates the restriction of small rotations between two successive increments. Both Total Lagrangian Formulation and Generalized Displacement Control Method are employed for analyzing the shells. Several numerical tests are performed to corroborate the accuracy and efficiency of the suggested approach.

Keywords: Geometrical nonlinear analysis; Composite materials; Axisymmetric shells; Shear deformation; Large rotation.

1. Introduction

Composite materials consist of two or more materials, which together exhibit the best properties of their constituents. These versatilities cause the composite materials to be extensively utilized in various engineering structures. Due to their high resistance, composite structures distort largely prior to the plastic deformation occurrence. As a result, these kinds of structures should be solved with the help of nonlinear geometric analysis techniques. Published papers clearly demonstrate that functionally graded and laminated fiber-reinforced composite materials have been widely employed in the modern shell structures.

The geometric nonlinear analysis of laminated composite shells was performed by Librescu [1] and Dennis and Palazotte [2]. To solve the spherical laminated shells under large deformations, Alwar and Narasimhan took advantage of virtual work principle [3]. By generalizing the first assumption of Love and Dannel's theory, Birman proposed an accurate method for analyzing the nonlinear behavior of laminated cylindrical shells [4]. In 1993, Chandrashekhara and Kumar studied the exact solutions of thick cylindrical shells with simple supports. In their work, shells were analyzed under axisymmetric loads [5]. Moreover, they suggested an approximate elastic behavior technique. A hierarchical p-version finite element formulation was applied in the geometric nonlinear analysis of composite shells by Liu and Surana [6]. Ziyaeifar and Elwi proposed a more accurate shear strain field through the thickness by deploying two new shape functions. Employing the finite element method and the Lagrangian formulation, they highlighted the merits of these shape functions [7].

Linear and nonlinear analyses of anisotropic shell structures were performed by Argyris et al. They used a 3-noded flat shell element with shear deformable capability, known as TRIC [8]. In another paper, Argyris et al. demonstrated the performance and accuracy of TRIC element in post buckling analysis of composites [9]. In 2000, Pinto Correia et al. utilized the higher-order theory to present a semi-analytical finite element model for solving laminated symmetric shells [10]. In that study, Fourier integration was employed for developing displacement and strain fields. Dumir et al. carried out static and

Published online November 25 2018

transient analysis to assess the behavior of laminated orthotropic symmetric shells under symmetric loads which was uniformly distributed. To find the solution, layers were considered to be polar orthotropic. Besides, they took advantage of the first-order shear deformation theory [11]. In another study, Pinto Correia et al. analyzed the laminated conical shell. Isoparametric elements and the higher-order shear deformation theory were used by these investigators [12].

In 2005, Santos et al. studied the bending, free vibration, and buckling of the shells of revolution made of laminated orthotropic elastic material by using 3D elasticity theory, semi-analytical finite element model, and Fourier series expansion in circumferential direction [13]. Wu et al. proposed 3D solution of the laminated conical shells under axisymmetric load patterns. To find the solution, they took advantage of the perturbation method [14]. Additionally, Smith analyzed the static deformation and the stress of the axisymmetric shells by applying the flexibility scheme. In that research work, the shell was reduced to ring section. The exact evaluation of the stress was utilized in circumferential direction of the rings. On the other hand, the distribution of stress in the meridional direction was assumed to be linear [15]. Reddy introduced a refined nonlinear theory of plates accounting for the von karman strains. In his study, parabolic transverse shear strains were assumed to vary through the thickness of the plates [16]. The same author presented a review of the theories for equivalent-single-layer and also layer-wise laminates [17].

Mantary et al. developed a new higher-order shear deformation theory for elastic laminated plates and shells [18]. The parabolic distribution of the transverse shear strains through the thickness was utilized in their formulation. They used the principle of the virtual work to derive the governing equations. Han et al. proposed an element for the nonlinear analysis of laminated shells based on a modified first-order shear theory [19]. Their element showed neither membrane nor shear locking problem. That behavior was accomplished by using natural co-ordinate-based higher-order transverse shear strains. Reddy and Liu developed a higher-order shear deformation theory for the analysis of laminated shells [20]. They presented exact solutions for deflections and natural frequencies of cross-ply shells. Noor et al. presented an analytical formulation for predicting the linear small deformation response of the laminated anisotropic shells of revolution. They used the Sanders-Budiansky shell theory, including the effects of both the transverse shear deformation and the laminated anisotropic material properties [21].

Sheinman et al. studied the nonlinear analysis of geometrically imperfect, thin, laminated circular cylindrical shells subjected to a uniform axial compression. They investigated the effect of stacking lamina on the responses [22]. Patel et al. employed the semi-analytical finite element approach to study the influence of ply-angle and number of circumferential waves on the pre/post-buckling response of the anti-symmetric angle-ply laminated circular conical shells [23]. In another paper, they investigated the post-buckling behavior of laminated shell of revolution with meridional curvature subjected to thermal and mechanical loads. They utilized a semi-analytical finite element approach based on the first-order shear deformation theory and the field consistency approach [24]. Cagdas developed a curved axisymmetric shell finite element based on the first-order shear deformation theory to analyze the linear stability of cross-ply laminated shells of revolution. A consistent thick shell theory is used in that formulation [25].

Wu and Chi presented an asymptotic theory for the analysis of laminated composite cylindrical shells under cylindrical bending based on the 3D nonlinear elasticity. They employed the perturbation method to decompose the 3D nonlinear theory into a series of 2D nonlinear theories for various orders [26]. Bhaskar and Varadan presented a displacement-base continuous isoparametric quadrilateral shell element for the analysis of laminated anisotropic shells of revolution [27]. Bhimaraddi et al. developed a shear deformable isoparametric quadrilateral shell element for the analysis of laminated shells of revolution. Parabolic shear strain variation was employed to obtain a more realistic variation for the transverse shear strain [28]. Chang and Sawamiphakdi presented a degenerated three-dimensional isoparametric element for conducting large deformation analysis of laminated anisotropic shells. The updated Lagrarangian formulation was used to derive the nonlinear geometric stiffness matrices [29]. Rezaiee-Pajand and Arabi proposed a 6-node triangular isoparametric shell element for the geometrically nonlinear analysis of laminates. They utilized the mixed interpolation technique to alleviate the shear and membrane locking problem [30]. Xu studied the buckling and post-buckling of the laminated cross-ply spherical cap under uniform normal pressure. Transverse shear deformations were included in derivation of governing equations [31]. Alankaya and Oktem performed static analysis of the cross-ply doubly-curved shell using a third order shear deformation theory [32]. The buckling analysis of a non-homogeneous orthotropic truncated conical shell under axial compression and external pressure is presented by Sofiyev and Kuruoglu [33]. Rezaiee-Pajand et al. developed a curved triangular element for nonlinear analysis. They took advantages of interpolation functions for strain fields to improve the element behavior [34].

In 2009, Santos et al. developed a semi analytical axisymmetric finite element model for studying free vibration of functionally graded cylindrical shells [35]. The nonlinear static and dynamic buckling analysis of functionally graded shallow spherical shells was performed by Bich et al. [36]. They took into account the von Karman-Donnel geometrical nonlinearity along with the classical shell theory for derivation of the governing equations. Bich and Tung presented an analytical formulation to study the nonlinear axisymmetric behavior of functionally graded shallow spherical shells under uniform external pressure [37]. In another work, Zozulya and Zhang utilized the Fourier series expansion and proposed a higher-order theory of functionally graded axisymmetric cylindrical shell [38]. In 2014, Viola et al. applied a two-dimensional unconstrained third-order shear deformation theory to investigate the behavior of functionally graded conical shells and panels [39]. They used the Generalized Differential Quadrature method to solve the derived partial differential equations. Arciniega and Reddy developed a tensor-based functionally graded shell finite element [40]. To mitigate the locking problems, the field variables were approximated using higher-order Lagrangian interpolation functions. Kar and Panda developed a mathematical model based on the higher order shear deformation theory for studying the nonlinear free vibration behavior of functionally graded spherical shells [41]. The three-dimensional analysis of functionally graded axisymmetric circular plates was performed employing mesh less method by Wu and Liu [42].

Based on the available literature, published technical articles on the topic of higher-order shear deformation theory of the composite shells are enormous. However, most of them are devoted to general shells. It is worth mentioning that only a few research works have dealt with the geometric nonlinear analysis of the composite axisymmetric shell by using 1-dimensional axisymmetric elements with large rotation capability. In fact, previous published papers took advantage of the higher-order shear deformation theory and the general shell element or the semi-analytical approach to solve the axisymmetric shell. As these structures have vast applications in industry, this paper is specifically devoted to the static analysis of composite axisymmetric shells. A1D axisymmetric element presented for isotropic material by Surana [43] is improved for geometrically nonlinear analysis of composite structures utilizing the higher-order shape functions along with the displacement field theory. To prove the capability of the authors' approach, several numerical samples will be solved. The obtained numerical solutions will be compared with the other researchers' results as well.

2. Finite element formulation

For the finite element modeling of the axisymmetric shell, an isoparametric 1D three-nodded element is deployed. This element is illustrated in Fig. 1. where curvilinear coordinates are presented by r and s. The geometry of the structure is defined as follows:

$$\boldsymbol{x} = \sum_{i=1}^{3} h_i(r)\boldsymbol{x}_i + \frac{1}{2}\sum_{i=1}^{3} h_i(r) s t_i \{F_i\}$$
$$F_i = \begin{Bmatrix} \cos\varphi_i \\ \sin\varphi_i \end{Bmatrix} \tag{1}$$

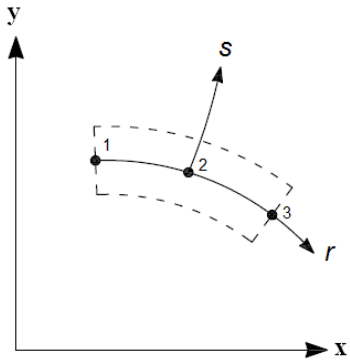

Fig. 1. Isoparametric 1D three-nodded element

where h_i and t_i are shape function and thickness of node i, respectively. The nodal variables and angle φ_i at i are demonstrated in Fig. 2.

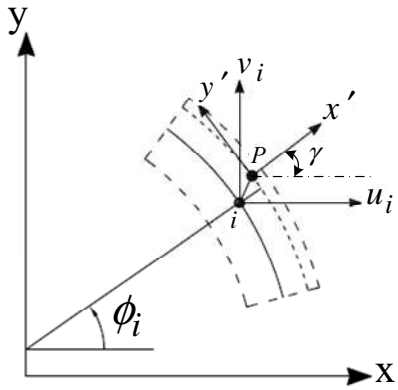

Fig. 2. Nodal variables and local coordinates

Based on these Figures, the displacement field of any arbitrary point P of the shell can be expressed as

$$\boldsymbol{u} = \sum_{i=1}^{3} h_i(r)\boldsymbol{u}_i + \frac{1}{2}\sum_{i=1}^{3} h_i(r) s t_i \left\{\overline{F}_i\right\} + \frac{1}{6}\sum_{i=1}^{3} h_i(r) s^3 t_i \left\{\overline{\overline{F}}_i\right\} \beta_i \tag{2}$$

$$\left\{\overline{F}_i\right\}=\begin{Bmatrix}\overline{F}_{ix}\\ \overline{F}_{iy}\end{Bmatrix}=\begin{Bmatrix}\cos\varphi_i\left(\cos\alpha_i-1\right)-\sin\varphi_i\sin\alpha_i\\ \sin\varphi_i\left(\cos\alpha_i-1\right)+\cos\varphi_i\sin\alpha_i\end{Bmatrix}$$
$$\left\{\overline{\overline{F}}_i\right\}=\begin{Bmatrix}\overline{\overline{F}}_{ix}\\ \overline{\overline{F}}_{iy}\end{Bmatrix}=\begin{Bmatrix}-\cos\varphi_i\sin\alpha_i-\sin\varphi_i\cos\alpha_i\\ -\sin\varphi_i\sin\alpha_i+\cos\varphi_i\cos\alpha_i\end{Bmatrix} \tag{3}$$

In these equations, the rotation angles of the vector normal to the mid plane are denoted by α and β. The shape function of node i is shown by $h_i(r)$. It should be noted that α represents the assumption of the first-order shear deformation theory (hereafter FSDT), while β involves the higher-order shear deformation term (hereafter HSDT). Take into consideration that the isoparametric coordinates are r and s. Stress-strain relations have the following appearance in the global coordinates:

$$\{\sigma\}=[Q]\{\varepsilon\} \tag{4}$$
$$[Q]=[T]\left[\overline{Q}\right][T]^T \tag{5}$$
$$[T]=\begin{bmatrix}c^2 & s^2 & -2sc & 0\\ s^2 & c^2 & 2sc & 0\\ sc & -sc & c^2-s^2 & 0\\ 0 & 0 & 0 & 1\end{bmatrix} \tag{6}$$
$$s=\sin(\gamma)\quad,\quad c=\cos(\gamma)$$

Here, the angle between coordinate x and x' is shown by γ. The coefficients of the constitutive matrix are given for two cases: Laminates and Functionally graded materials (FGM). These parameters are presented in material coordinates for each orthotropic lamina and FGM, respectively:

$$\begin{cases}\bar{Q}_{11}=\dfrac{E_1}{1-\nu_{12}\nu_{21}},\bar{Q}_{12}=\bar{Q}_{21}=\dfrac{E_1\nu_{21}}{1-\nu_{12}\nu_{21}}\\ \bar{Q}_{14}=\bar{Q}_{41}=\dfrac{E_1\nu_{31}}{1-\nu_{12}\nu_{21}},\bar{Q}_{22}=\dfrac{E_2}{1-\nu_{12}\nu_{21}} & \textit{Lamina}\\ \bar{Q}_{24}=\bar{Q}_{42}=\dfrac{E_2\nu_{32}}{1-\nu_{12}\nu_{21}},\bar{Q}_{33}=G_{12},\bar{Q}_{44}=\dfrac{E_3}{1-\nu_{12}\nu_{21}}\end{cases}$$
$$\begin{cases}\bar{Q}_{11}=\bar{Q}_{22}=\bar{Q}_{44}=\dfrac{E(s)}{1-\nu^2},\bar{Q}_{33}=\dfrac{E(s)}{2(1+\nu)}\\ \bar{Q}_{12}=\bar{Q}_{21}=\bar{Q}_{24}=\bar{Q}_{42}=\bar{Q}_{14}=\bar{Q}_{41}=\dfrac{E(s)\nu}{1-\nu^2} & FG\\ E(s)=E_m+(E_c-E_m)\left(\dfrac{s}{2}+\dfrac{1}{2}\right)^n\end{cases} \tag{7}$$

In which E, ν, and G represent the engineering constants. Moreover, the subscripts m and c stands for to the metal and ceramic constituents. The volume fraction exponent is shown by *n*. It is worth mentioning that in FG material, Poisson's ratio is considered to be constant through the thickness.

In global coordinates, the strains for an axisymmetric shell have the following form:

$$\{\varepsilon\}=\begin{Bmatrix}u_{,x} & +\dfrac{1}{2}\left[\left(u_{,x}\right)^2+\left(v_{,x}\right)^2\right]\\ v_{,y} & +\dfrac{1}{2}\left[\left(u_{,y}\right)^2+\left(v_{,y}\right)^2\right]\\ u_{,y}+v_{,x} & +u_{,x}u_{,y}+v_{,x}v_{,y}\\ \dfrac{u}{x} & +\dfrac{1}{2}\left(\dfrac{u}{x}\right)^2\end{Bmatrix} \tag{8}$$

In this case, u/x corresponds to the strain in circumferential direction. Moreover, x represents the projection of an arbitrary point position in radial direction. The strains can be divided into a linear and nonlinear part as

$$\{\varepsilon_l\}=\begin{bmatrix}1&0&0&0&0\\0&0&0&1&0\\0&1&1&0&0\\0&0&0&0&1\end{bmatrix}\begin{Bmatrix}u_{,x}\\v_{,x}\\u_{,y}\\v_{,y}\\\dfrac{u}{x}\end{Bmatrix}=[H_l]\{\theta\} \tag{9}$$

$$\{\varepsilon_{nl}\}=\frac{1}{2}\begin{bmatrix}u_{,x}&v_{,x}&0&0&0\\0&0&u_{,y}&v_{,y}&0\\u_{,y}&v_{,y}&u_{,x}&v_{,x}&0\\0&0&0&0&\dfrac{u}{x}\end{bmatrix}\begin{Bmatrix}u_{,x}\\v_{,x}\\u_{,y}\\v_{,y}\\\dfrac{u}{x}\end{Bmatrix}=\frac{1}{2}[H_{nl}]\{\theta\} \tag{10}$$

$$\{\theta\}=\begin{Bmatrix}u_{,x}\\v_{,x}\\u_{,y}\\v_{,y}\\\dfrac{u}{x}\end{Bmatrix} \tag{11}$$

At point i, the variation of the nodal variable can be expressed as follows:

$$\delta\{d_i\}=\begin{Bmatrix}\delta u_i\\\delta v_i\\\delta\alpha_i\\\delta\beta_i\end{Bmatrix} \tag{12}$$

Using Eqs. (9) and (10), the variation of the linear and nonlinear strain is written in terms of nodal variable $\{d\}$ as follows:

$$\delta\{\varepsilon_l\}=[H_l]\delta\{\theta\}=[H_l][G]\delta\{d\}=[B_l]\delta\{d\} \tag{13}$$

$$\delta\{\varepsilon_{nl}\}=\frac{1}{2}\delta[H_{nl}]\{\theta\}+\frac{1}{2}[H_{nl}]\delta\{\theta\}=[H_{nl}]\delta\{\theta\}=[H_{nl}][G]\delta\{d\}=[B_{nl}]\delta\{d\} \tag{14}$$

$$\delta\{\varepsilon\}=[B_l+B_{nl}]\delta\{d\}=\left[[H_l]+[H_{nl}]\right][G]\delta\{d\}=[B]\delta\{d\} \tag{15}$$

The entries of matrix $[G]$ are presented in Appendix A. The equation of static equilibrium has the following shape:

$$\{\psi\}=\{R\}-\int_V[B]^T\{\sigma\}dV=\{R\}-\{P\} \tag{16}$$

where $\{R\}$ and $\{P\}$ denote the vectors of external and internal forces, respectively. Since Eq. (16) cannot be solved directly for deflections, an incremental equation of equilibrium should be derived. This equation has the following form:

$$\delta\{\psi\}=\delta\{R\}-\int_V\delta[B]^T\{\sigma\}dV-\int_V[B]^T\delta\{\sigma\}dV \tag{17}$$

By using the relation $\delta\{\sigma\}=[Q]\delta\{\varepsilon\}$, Eq.(17) can be rewritten as follows:

$$\delta\{\psi\}=\delta\{R\}-\int_V\delta[B]^T\{\sigma\}dV-[K_l]\delta\{d\} \tag{18}$$

$$[K_l]=\int_V [B]^T [Q][B]dV \tag{19}$$

Inserting Eq. (15) into integral of the Eq. (18) leads to the geometric stiffness matrices. These matrices have the following appearance:

$$\int_V \delta[B]^T \{\sigma\}dV =\int_V \left(\delta[B_l]^T +\delta[B_{nl}]^T\right)\{\sigma\}dV =\int_V \left(\delta[G]^T [H_l]^T +\delta[G]^T [H_{nl}]^T +[G]^T \delta[H_{nl}]^T\right)\{\sigma\}dV \tag{20}$$

$$\int_V [G]^T \delta[H_{nl}]^T \{\sigma\}dV =[K_{G1}]\delta\{d\} \tag{21}$$

It can be easily shown that $\delta[H_{nl}]^T \{\sigma\}=[S][G]\delta\{d\}$. Using this equation, the following expression is achieved for$[K_{G1}]$:

$$[K_{G1}]=\left[\int_V [G]^T [S][G]dV\right] \tag{22}$$

$$[S]=\begin{bmatrix}\sigma_x I_2 & \tau_{xy} I_2 & 0\\ \tau_{xy} I_2 & \sigma_y I_2 & 0\\ 0 & 0 & \sigma_Z\end{bmatrix} \tag{23}$$

In this relation, I_2 is a 2×2 unit matrix. The next equation is held for$[K_{G2}]$:

$$\int_V \delta[G]^T [H_l]^T \{\sigma\}dV =[K_{G2}]\delta\{d\} \tag{24}$$

$$[H_l]^T \{\sigma\}=\begin{bmatrix}1&0&0&0\\0&0&1&0\\0&0&1&0\\0&1&0&0\\0&0&0&1\end{bmatrix}\begin{Bmatrix}\sigma_x\\ \sigma_y\\ \tau_{xy}\\ \sigma_z\end{Bmatrix}=\{\hat{\sigma}\} \tag{25}$$

Treating $\{\hat{\sigma}\}$ as constant values, the following equalities can be written:

$$\delta[G]^T \{\hat{\sigma}\}=\delta\left[[G]^T \{\hat{\sigma}\}\right]=\delta\begin{bmatrix}G_{11}&0&G_{31}&0&G_{51}\\0&G_{22}&0&G_{42}&0\\G_{13}&G_{23}&G_{33}&G_{43}&G_{53}\\G_{14}&G_{24}&G_{34}&G_{44}&G_{54}\end{bmatrix}\begin{Bmatrix}\sigma_x\\ \tau_{xy}\\ \tau_{xy}\\ \sigma_y\\ \sigma_z\end{Bmatrix}=\delta\begin{Bmatrix}N_1\\N_2\\N_3\\N_4\end{Bmatrix}=\delta\{N\} \tag{26}$$

For each node i, the variation of $\{N\}$ can be found. It should be noted, if both N_1 and N_2 are constants, the following expressions are held:

$$\{\delta N_i\}=\begin{Bmatrix}0\\0\\\delta N_{3i}\\\delta N_{4i}\end{Bmatrix}$$

$$\delta N_{3i} =P_{3i}\frac{\partial^2 \overline{F}_{ix}}{\partial\alpha_i^2}\delta\alpha_i +Q_{3i}\frac{\partial^2 \overline{F}_{iy}}{\partial\alpha_i^2}\delta\alpha_i \tag{27}$$

$$\delta N_{4i} =\overline{P}_{3i}\frac{\partial^2 \overline{F}_{ix}}{\partial\alpha_i^2}\delta\beta_i +\overline{Q}_{3i}\frac{\partial^2 \overline{F}_{iy}}{\partial\alpha_i^2}\delta\beta_i$$

By using Eqs. (26) and (27), $\left[K_{G2}\right]$ is obtained as follows:

$$\left[K_{G2}^{ii}\right]=\begin{bmatrix}0 & 0 & 0 & 0\\ 0 & 0 & 0 & 0\\ 0 & 0 & \left(K_{G2}^{ii}\right)_{3,3} & 0\\ 0 & 0 & 0 & \left(K_{G2}^{ii}\right)_{4,4}\end{bmatrix} \quad , \quad j\neq k \quad , \quad 1\le j,k\le 3 \quad , \quad 1\le i\le 3 \tag{28}$$

$$\left[K_{G2}^{jk}\right]=[0]$$

$$\left(K_{G2}^{ii}\right)_{3,3}=\int_V\left(P_{3i}\frac{\partial^2\overline{F}_{ix}}{\partial\alpha_i^2}+Q_{3i}\frac{\partial^2\overline{F}_{iy}}{\partial\alpha_i^2}\right)dV \tag{29}$$

$$\left(K_{G2}^{ii}\right)_{4,4}=\int_V\left(\overline{P}_{3i}\frac{\partial^2\overline{F}_{ix}}{\partial\alpha_i^2}+\overline{Q}_{3i}\frac{\partial^2\overline{F}_{iy}}{\partial\alpha_i^2}\right)dV \tag{30}$$

In a similar manner, the next expressions can be obtained for $\left[K_{G3}\right]$:

$$\int_V\delta[G]^T\left[H_{nl}\right]^T\{\sigma\}dV=\left[K_{G3}\right]\delta\{d\} \tag{31}$$

$$\left[K_{G3}^{ii}\right]=\begin{bmatrix}0 & 0 & 0 & 0\\ 0 & 0 & 0 & 0\\ 0 & 0 & \left(K_{G3}^{ii}\right)_{3,3} & 0\\ 0 & 0 & 0 & \left(K_{G3}^{ii}\right)_{4,4}\end{bmatrix} \quad , \quad j\neq k \quad , \quad 1\le j,k\le 3 \quad , \quad 1\le i\le 3 \tag{32}$$

$$\left[K_{G3}^{jk}\right]=[0]$$

$$\left(K_{G3}^{ii}\right)_{3,3}=\int_V\left(\hat{P}_{3i}\frac{\partial^2\overline{F}_{ix}}{\partial\alpha_i^2}+\hat{Q}_{3i}\frac{\partial^2\overline{F}_{iy}}{\partial\alpha_i^2}\right)dV \tag{33}$$

$$\left(K_{G3}^{ii}\right)_{4,4}=\int_V\left(\tilde{P}_{3i}\frac{\partial^2\overline{F}_{ix}}{\partial\alpha_i^2}+\tilde{Q}_{3i}\frac{\partial^2\overline{F}_{iy}}{\partial\alpha_i^2}\right)dV \tag{34}$$

It should be added that the value of P_{3i} ,Q_{3i} , $\overline{P}_{3i}$, $\overline{Q}_{3i}$, $\hat{P}_{3i}$, $\hat{Q}_{3i}$, $\tilde{P}_{3i}$, and $\tilde{Q}_{3i}$ are given in Appendix B.

Based on the presented formulation, a computer code is developed. To find the answers, the incremental equation of static equilibrium is solved by using the Generalized Displacement Control Method (GDCM) (Leon et al. [44]). The incremental-iterative procedure is given in Appendix C.

3. Numerical study

In this section, the proposed approach is applied to analyze several sample structures. The numerical examples are presented in three parts. To validate the accuracy of the responses, the obtained results are compared with those found by the other researchers at first. In this way, the ability of the suggested formulation is assessed. In the second part, the structures are analyzed by the presented 1-D axisymmetric element and also by using a doubly curved triangular 6-nodded shell element proposed in [30]. This comparison study reveals the method accuracy. More important, when the present technique is used in the analysis, it extremely demonstrates the saving time. Part three demonstrates the nonlinear analysis of functionally graded axisymmetric shells for various power law indexes. Regarding the effects of shear deformation in composite axisymmetric shells, the responses are calculated for two cases, namely, FSDT and HSDT.

3.1 Part 1

3.1.1 Annular plate

The deformation of the ring-shaped plate illustrated in Fig. 3b is computed. A finite element model of the plate using 3 three-node axisymmetric elements is shown in Fig. 3c.

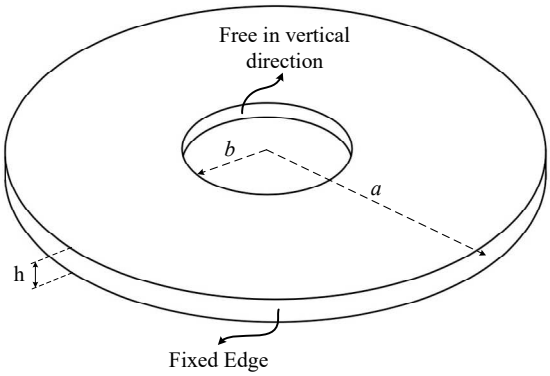

(a) 3D view

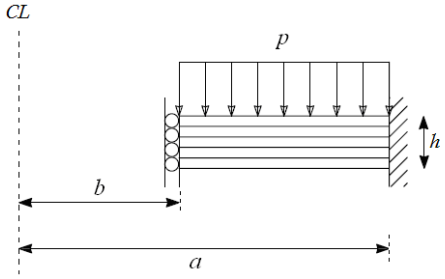

(b) Geometry description

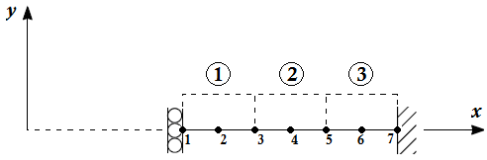

(c) Finite element discretization

Fig. 3. Annular plate

This structure was previously analyzed by Dumir et al. [11]. The aforementioned structure has five orthotropic layers. The thickness of these layers is the same. The plate is subjected to the uniformly distributed load. Three different ratios of the radius to thickness, 10, 20, and 100, are studied. The external edge of the plate is fixed and the inner edge is free in the direction of the deflection. The layers are arranged with respect to the radial direction (0/90/0/90/0). The material properties are given below:

$$\psi = E_1/E_2 = 3,40 \quad , \quad G/E_2 = 0.5 \quad , \quad \upsilon_{12} = 0.25$$

In Fig. 4, dimensionless diagrams are utilized to show the results obtained from the authors' technique against the method presented in [11]. It is worth mentioning that the first-order shear deflection theory was applied in the latter approach. It is obvious that the shear deformation plays an important role in plates with a low ratio of the radius to thickness. Moreover, this deformation has more effect on the behavior of plates made of the orthotropic material with greater modular ratio ψ. Based on FSDT and HSDT, the deflection of the laminated plate for $pa^4/E_1h^4 = 130$ is computed by using the proposed formulation. The results are shown in Table 1. Clearly, the displacement corresponding to the HSDT is less than that of FSDT.

Table 1. Dimensionless displacement of the ring-shaped plate

ψ	$a/h = 100$		$a/h = 20$		$a/h = 10$	
	FSDT	HSDT	FSDT	HSDT	FSDT	HSDT
3	1.475	1.474	1.538	1.531	1.598	1.584
40	1.683	1.677	1.876	1.867	1.937	1.931

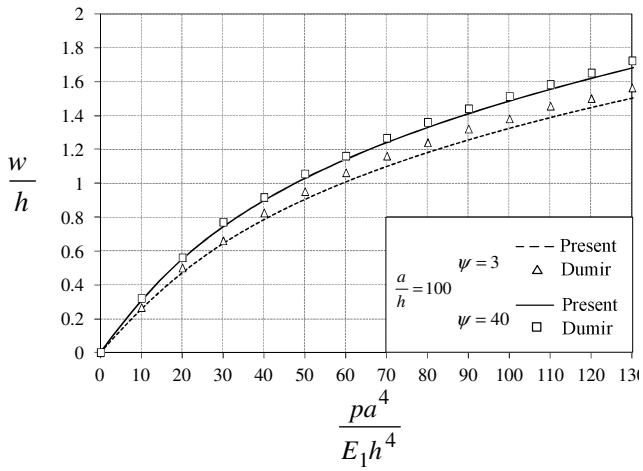

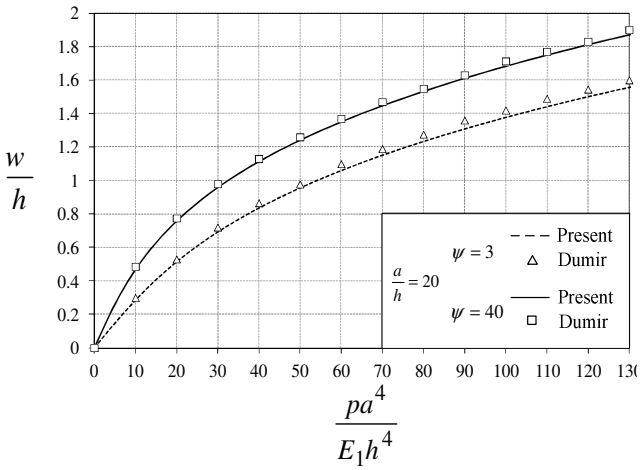

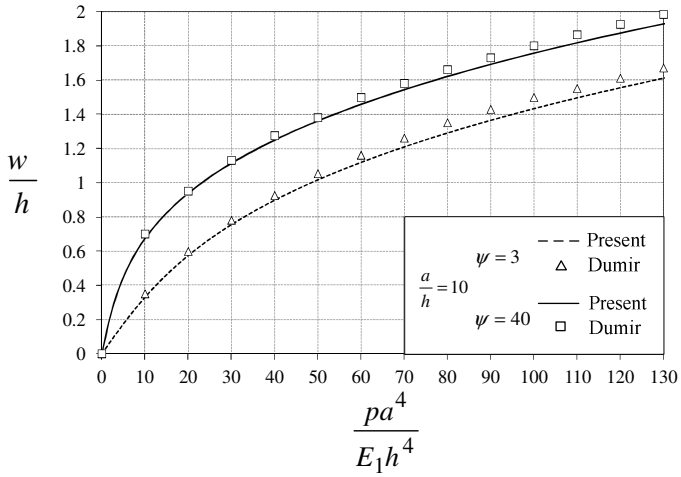

Fig. 4. Deflection of the annular plate

3.1.2 Cylindrical shell

A one-layer glass-epoxy cylinder subjected to a uniform internal pressure and its corresponding finite element model utilizing 10 three-node axisymmetric elements are shown in Fig. 5. The cylinder is clamped at both ends. Radius, length, and thickness of the shell are R=20, L=20, and h=1, respectively. The material properties are characterized by the following elastic constants:

$$E_1 = 7500 \quad , \quad E_2 = 2000 \quad , \quad \upsilon_{12} = 0.25 \quad , \quad G = 625$$

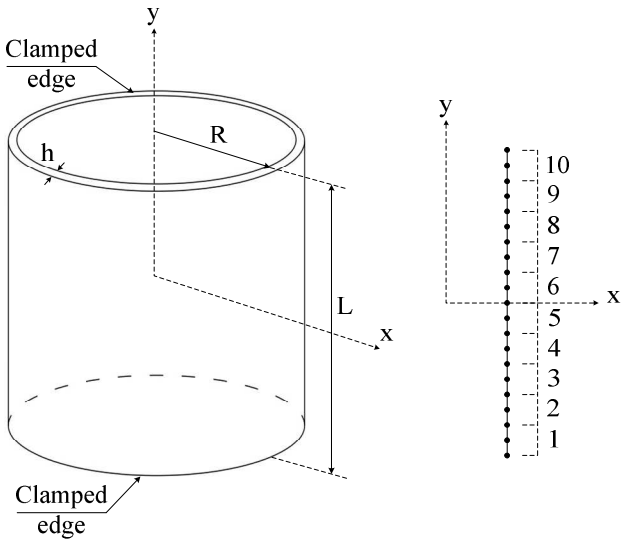

Fig. 5. Cylindrical shell under internal pressure and its corresponding meshing

As can be seen, Fig 6 contains the plot of center deflection of the shell versus the internal pressure, for the present formulation and the work done in [29]. The agreement between the present and reference results is very good. Table 2 shows the difference between the solutions when the FSDT and HSDT models are used.

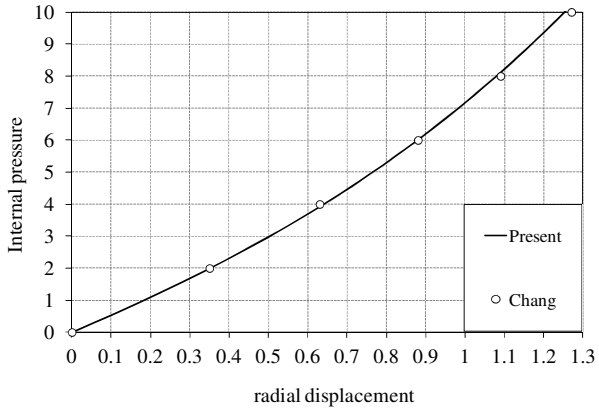

Fig. 6. Radial deflection of cylindrical shell under internal pressure

Table 2. Radial displacement versus internal pressure

Internal Pressure	HSDT	FSDT
2	0.3496	0.3490
4	0.6386	0.6380
6	0.8765	0.8759
8	1.0771	1.0766
10	1.2504	1.2500

3.1.3 Spherical cap

In this problem, the post-buckling response of a clamped cross-ply spherical cap which has five layers is investigated. The cross-section of spherical cap and its finite element discretization using 10 three-node axisymmetric elements is shown in Figs. 7(a), (b). The shell is under a uniform normal pressure. The elastic constants have the following relations:

$$E_1/E_2 = 10 \quad , \quad G/E_2 = 0.333 \quad , \quad \upsilon_{12} = 0.22$$

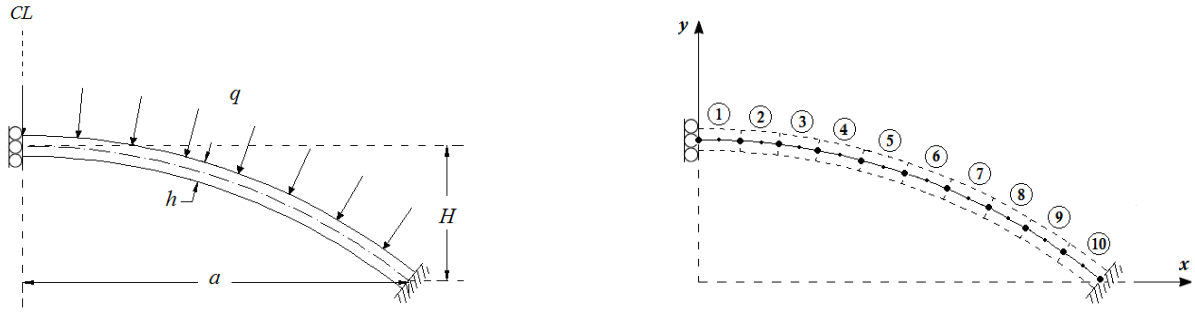

(a) Geometry description (b) Finite element discretization

Fig. 7. Spherical shell

The response curves of spherical shell for values of $H/a = 0.1$ and $a/h = 15$ are compared in Fig. 8 with the result obtained by Xu [31]. The comparisons between the results indicate that dimensionless displacements of the HSDT method are more than FSDT.

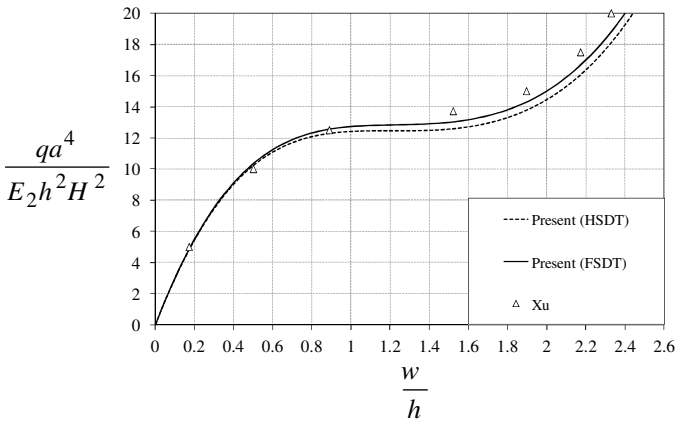

Fig. 8. Cylindrical shell under internal pressure and its corresponding meshing

3.2 Part 2

3.2.1 Conical laminated shell

A conical three-layer shell is shown in Fig. 9. The shell is modeled using 10 three-node axisymmetric elements. This structure is analyzed under the ring load. In the larger span, the shell's supports are fixed in the vertical direction. The material properties and structure's geometry are expressed in the following form:

$$E_1/E_2 = 3 \ , \ G/E_2 = 0.6 \ , \ \upsilon = 0.3 \ , \ E_2 = 11000 \ , \ R_1/R_2 = 3 \ , \ R_1/h = 15 \ , \ R_1 = 3 \ , \ H = 0.5$$

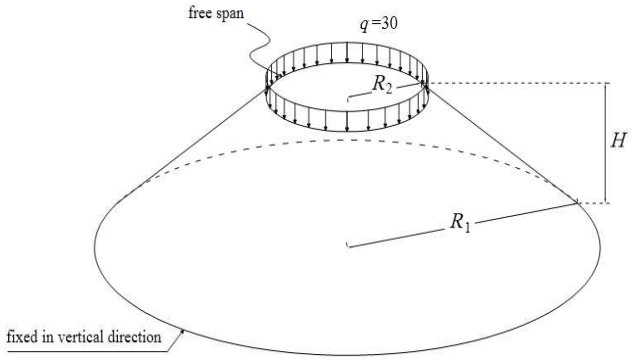

Fig. 9. Conical shell

The nonlinear analysis of the shell is carried out using the present 1-D axisymmetric shell element and $12\times12\times2$ doubly curved triangular 6-nodded shell element proposed in [30]. The deflection of the mid plane at free span versus the load factor is plotted in Fig. 10, for two cross-ply laminates with schemes (0/90/0) and (90/0/90). It should be noted that the average time of the analysis for the present formulation is about 1/200 of the general shell formulation. This shows an extremely time saving merit, when the present scheme is utilized.

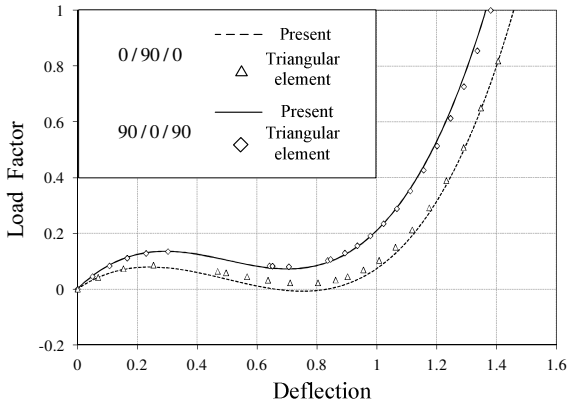

Fig. 10. Deflection of conical shell under ring load

The downward deflections of the cutout for FSDT and HSDT methods are listed in Table 3. Comparing the responses of the nonlinear analysis reveals that the vertical displacement of conical shell using HSDT method is greater than FSDT.

Table 3. The downward deflection of conical shell

Load Factor	[0/90/0]		[90/0/90]	
	FSDT	HSDT	FSDT	HSDT
0.2	1.1232	1.1247	0.9930	0.9947
0.4	1.2407	1.2420	1.1345	1.1360
0.6	1.3302	1.3322	1.2299	1.2313
0.8	1.3984	1.3995	1.3035	1.3047
1.0	1.4586	1.4594	1.3659	1.3669

3.2.2 Cross-ply spherical shell

The cross-ply spherical shell, with stacking sequences (0/90/0) and (90/0/90), is analyzed. The shell has a 18^o circular cutout at its pole and is loaded by a ring force at the cutout. The shell and its geometric descriptions are shown in Fig. 11. A finite element model adopting 10 three-node elements is applied. The material data used for this analysis has the following values:

$$E_1 = 6\times10^7,\quad E_2 = 2\times10^7,\quad G = 1.125\times10^7,\quad \upsilon_{12} = 0.3$$

As shown, Fig. 12 plots the load factor against the downward deflection of the cutout for the present shell element. The results of nonlinear formulation utilizing $12\times12\times2$ doubly curved triangular shell element are also included in Fig. 12 for comparison. It is worth mentioning that the average time to reach the solution for the general shell formulation is about 287 times more than the present element. This is the advantage of using the present 1-D axisymmetric shell element instead of the general shell element.

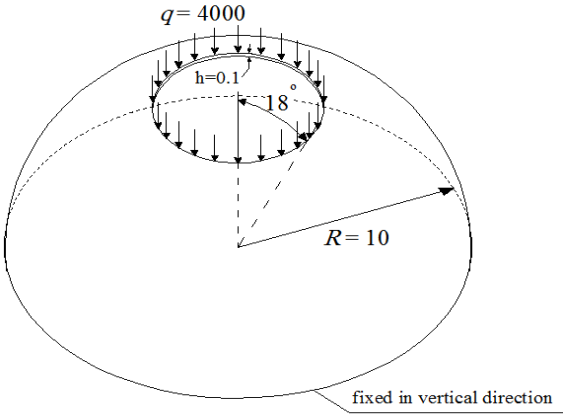

Fig. 11. Spherical shell with cutout

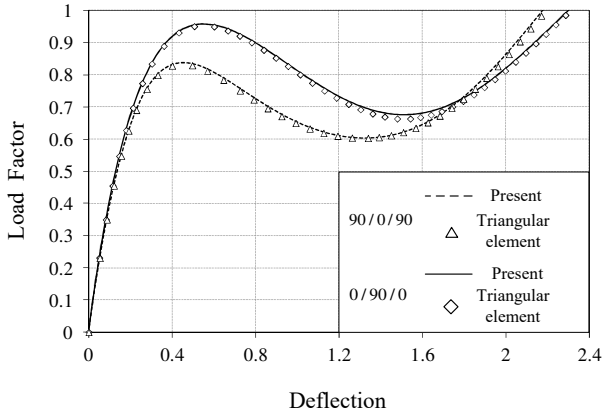

Fig. 12. Deflection of spherical shell under ring load

FSDT and HSDT results are presented in Table 4 for two lamination sequences, namely, [0/90/0] and [90/0/90]. According to the Table 4, the spherical shell undergoes a lower displacement when utilizing the higher-order shear deformation theory.

Table 4. The deflection of spherical shell

Load	[0/90/0]		[90/0/90]		Load	[0/90/0]		[90/0/90]	
Factor	FSDT	HSDT	FSDT	HSDT	Factor	FSDT	HSDT	FSDT	HSDT
0.2	0.0437	0.0437	0.0455	0.0455	0.8	1.0145	1.0316	0.6025	0.6250
0.4	0.0974	0.0973	0.1023	0.1022	0.8	1.9737	1.9606	1.9236	1.9085
0.6	0.1683	0.1681	0.1792	0.1788	1.0	2.3101	2.2986	2.1915	2.1755
0.8	0.2758	0.2743	0.3336	0.3282					

3.3 Part 3

3.3.1 Conical FG shell

The conical shell which previously analyzed in sample 1 of part 2 is investigated. The material properties for ceramic and metal are given as

$$E_m = 7\times10^7 \quad , \quad E_c = 1.51\times10^8 \quad , \quad \upsilon = 0.3$$

The maximum applied load is equal to 30000. The load-deflection curves are illustrated for the different volume fraction exponent in Fig.13. It is worth mentioning that fully ceramic and metal behavior is achieved as $n \to 0$ and $n \to \infty$, respectively.

The maximum downward deflection of the cutout for FSDT and HSDT methods is inserted for the different volume fraction exponent in Table 5.

Table 5. Maximum deflection of functionally graded conical shell

n	FSDT	HSDT
0.0	1.0039	1.0038
0.2	1.0228	1.0213
0.5	1.0421	1.0410
5.0	1.0970	1.0981
10.0	1.1106	1.1157
100.0	1.1371	1.1406

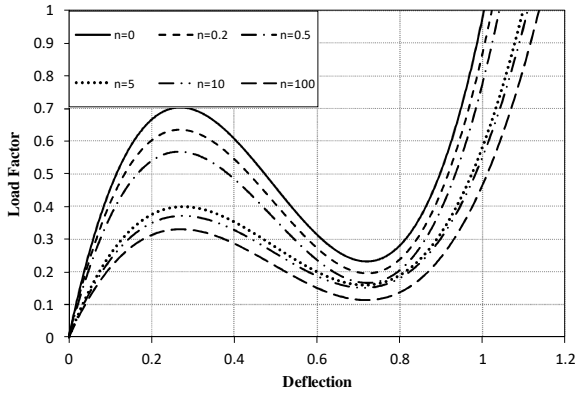

Fig. 13. Load-Deflection curves of conical shell for different volume fraction exponent

3.3.2 Spherical FG shell

A functionally graded spherical shell with cutout is analyzed in this section. The geometrical data is as those presented in sample 2 of part 2. The material properties for ceramic and metal have the following values:

$$E_m = 7\times10^7 \quad , \quad E_c = 1.51\times10^8 \quad , \quad \upsilon = 0.3$$

The load applied at the cutout is incrementally increased up to 20000. The deflection versus the load factor for various amounts of the volume fraction exponent are shown in Fig. 14.

The maximum vertical displacements, which are obtained by FSDT and HSDT methods, are compared for the various volume fraction exponents in Table 6.

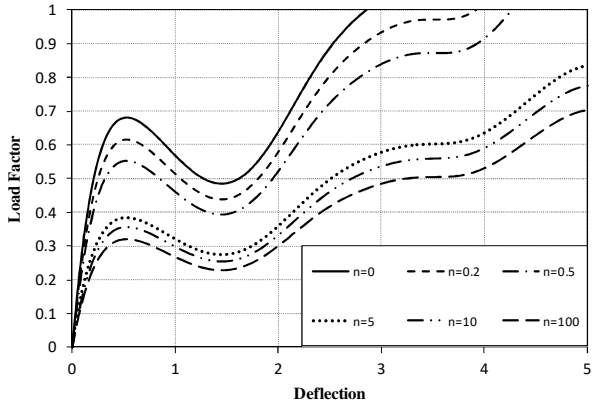

Fig. 14. Equilibrium path of spherical shell for various amounts of volume fraction exponent

Table 6. Maximum vertical displacement of functionally graded spherical shell

n	FSDT	HSDT
0.0	2.8510	2.8282
0.2	3.9123	3.8546
0.5	4.2672	4.2508
5.0	6.5254	6.5062
10.0	6.7732	6.7583
100.0	8.5150	8.5183

4. Conclusions

The finite element method is a very powerful scheme for solving the composite structures. In the present study, with the help of this method, the axisymmetric shells were analyzed using the authors' technique. In the laminated case, the shell's layers were assumed to be orthotropic. A 1D three nodded axisymmetric shell element was utilized. Higher-order shape functions and a large rotation technique were deployed in the formulation. The effects of lamination sequences on the structural responses were studied as well. Moreover, the various power law indexes were utilized to investigate the behavior of functionally graded shells. Comparing the results of the schemes of this study with other researchers' approaches proved the high ability of the suggested formulation in modeling the composite axisymmetric shells. Furthermore, a comparison for the average time to reach the solutions was made between the present element and a doubly curved shell element in laminated structures. By using the present formulation, the time of the analysis is enormously reduced with no loss of accuracy.

Conflict of Interest

The authors declare no conflict of interest.

Nomenclature

$[B]$	Matrix relating incremental nodal displacements to the incremental Green's strains	r, s	Curvilinear coordinates
$[B_l]$	Matrix relating incremental nodal displacements to the incremental linear strains	u, v	Deflection in the global x and y directions
$[B_{nl}]$	Matrix relating incremental nodal displacements to the incremental nonlinear strains	u_i, v_i	Deflection at node i
$\{d\}$	Generalized nodal displacement	x, y	Global Cartesian directions
h_i	Shape function for node i	α_i, β_i	Rotation degrees of freedom at node i
$[J]$	Jacobian matrix	$\delta\{d\}$	Generalized nodal displacement
$[J]^{-1}$	Inverse of the Jacobian matrix	$\{\varepsilon\}$	Global Green strain vectors
$[K_l], [K_{G1}], [K_{G2}], [K_{G3}]$	Element stiffness matrices	$\{\sigma\}$	Global Piola Kirchhoff stress vectors
$\{P\}$	Generalized internal force vector	φ_i	Angle at node i
$[Q]$	Elasticity matrix	$\{\psi\}$	Vector of residuals
$\{R\}$	Generalized external load vector		

Appendix A

The entries of matrix G have the following shapes:

$$G_{11} = \bar{A}_{11} \sum_{i=1}^{3} \frac{\partial h_i}{\partial r}$$

$$G_{12} = G_{21} = 0$$

$$G_{14} = \bar{A}_{11} \sum_{i=1}^{3} \frac{\partial h_i}{\partial r} \frac{s^3 t_i}{6} \frac{\partial \bar{F}_{ix}}{\partial \alpha_i} + \bar{A}_{12} \sum_{i=1}^{3} h_i \frac{s^2 t_i}{2} \frac{\partial \bar{F}_{ix}}{\partial \alpha_i}$$

$$G_{22} = \bar{A}_{11} \sum_{i=1}^{3} \frac{\partial h_i}{\partial r}$$

$$G_{23} = \bar{A}_{11} \sum_{i=1}^{3} \frac{\partial h_i}{\partial r} \frac{s t_i}{2} \frac{\partial \bar{F}_{iy}}{\partial \alpha_i} + \bar{A}_{12} \sum_{i=1}^{3} h_i \frac{t_i}{2} \frac{\partial \bar{F}_{iy}}{\partial \alpha_i}$$

$$G_{24} = \bar{A}_{11} \sum_{i=1}^{3} \frac{\partial h_i}{\partial r} \frac{s^3 t_i}{6} \frac{\partial \bar{F}_{iy}}{\partial \alpha_i} + \bar{A}_{12} \sum_{i=1}^{3} h_i \frac{s^2 t_i}{2} \frac{\partial \bar{F}_{iy}}{\partial \alpha_i}$$

$$G_{31} = \bar{A}_{21} \sum_{i=1}^{3} \frac{\partial h_i}{\partial r}$$

$$G_{32} = G_{41} = 0$$

$$G_{33} = \bar{A}_{21} \sum_{i=1}^{3} \frac{\partial h_i}{\partial r} \frac{s t_i}{2} \frac{\partial \bar{F}_{ix}}{\partial \alpha_i} + \bar{A}_{22} \sum_{i=1}^{3} h_i \frac{t_i}{2} \frac{\partial \bar{F}_{ix}}{\partial \alpha_i}$$

$$G_{34} = \bar{A}_{21} \sum_{i=1}^{3} \frac{\partial h_i}{\partial r} \frac{s^3 t_i}{6} \frac{\partial \bar{F}_{ix}}{\partial \alpha_i} + \bar{A}_{22} \sum_{i=1}^{3} h_i \frac{s^2 t_i}{2} \frac{\partial \bar{F}_{ix}}{\partial \alpha_i}$$

$$G_{42} = \bar{A}_{21} \sum_{i=1}^{3} \frac{\partial h_i}{\partial r}$$

$$G_{43} = \bar{A}_{21} \sum_{i=1}^{3} \frac{\partial h_i}{\partial r} \frac{s t_i}{2} \frac{\partial \bar{F}_{iy}}{\partial \alpha_i} + \bar{A}_{22} \sum_{i=1}^{3} h_i \frac{t_i}{2} \frac{\partial \bar{F}_{iy}}{\partial \alpha_i}$$

$$G_{44}=\bar{A}_{21}\sum_{i=1}^{3}\frac{\partial h_i}{\partial r}\frac{s^3t_i}{6}\frac{\partial \overline{F}_{iy}}{\partial \alpha_i}+\bar{A}_{22}\sum_{i=1}^{3}h_i\frac{s^2t_i}{2}\frac{\partial \overline{F}_{iy}}{\partial \alpha_i}$$

$$G_{51}=\sum_{i=1}^{3}\frac{h_i}{x}$$

$$G_{52}=0$$

$$G_{53}=\sum_{i=1}^{3}\frac{h_i}{x}\frac{st_i}{2}\frac{\partial \overline{F}_{ix}}{\partial \alpha_i}$$

$$G_{54}=\sum_{i=1}^{3}\frac{h_i}{x}\frac{s^3t_i}{6}\frac{\partial \overline{F}_{ix}}{\partial \alpha_i}$$

In these equations, $\bar{A}_{11}$, $\bar{A}_{12}$, $\bar{A}_{21}$ and $\bar{A}_{22}$ are the entries of the inverse of the below Jacobbian matrix.

$$[J]=\begin{bmatrix}\frac{\partial x}{\partial r} & \frac{\partial y}{\partial r}\\ \frac{\partial x}{\partial s} & \frac{\partial y}{\partial s}\end{bmatrix}\Rightarrow[J]^{-1}=\begin{bmatrix}\bar{A}_{11} & \bar{A}_{12}\\ \bar{A}_{21} & \bar{A}_{22}\end{bmatrix}$$

Appendix B

In the below lines, the value of P_{3i} ,Q_{3i} ,$\overline{P}_{3i}$, $\overline{Q}_{3i}$, $\hat{P}_{3i}$, $\hat{Q}_{3i}$, $\tilde{P}_{3i}$ and $\tilde{Q}_{3i}$ are given:

$$P_{3i}=\left[\left(\bar{A}_{11}\frac{\partial h_i}{\partial r}\frac{st_i}{2}+\bar{A}_{12}\frac{h_it_i}{2}\right)\sigma_x+\left(\bar{A}_{21}\frac{\partial h_i}{\partial r}\frac{st_i}{2}+\bar{A}_{22}\frac{h_it_i}{2}\right)\tau_{xy}+\frac{h_i}{x}\frac{st_i}{2}\sigma_y\right]$$

$$Q_{3i}=\left[\left(\bar{A}_{11}\frac{\partial h_i}{\partial r}\frac{st_i}{2}+\bar{A}_{12}\frac{h_it_i}{2}\right)\tau_{xy}+\left(\bar{A}_{21}\frac{\partial h_i}{\partial r}\frac{st_i}{2}+\bar{A}_{22}\frac{h_it_i}{2}\right)\sigma_y\right]$$

$$\overline{P}_{3i}=\left[\left(\bar{A}_{11}\frac{\partial h_i}{\partial r}\frac{s^3t_i}{6}+\bar{A}_{12}h_i\frac{s^2t_i}{2}\right)\sigma_x+\left(\bar{A}_{21}\frac{\partial h_i}{\partial r}\frac{s^3t_i}{6}+\bar{A}_{22}h_i\frac{s^2t_i}{2}\right)\tau_{xy}+\frac{h_i}{x}\frac{s^3t_i}{6}\sigma_y\right]$$

$$\overline{Q}_{3i}=\left[\left(\bar{A}_{11}\frac{\partial h_i}{\partial r}\frac{s^3t_i}{6}+\bar{A}_{12}h_i\frac{s^2t_i}{2}\right)\tau_{xy}+\left(\bar{A}_{21}\frac{\partial h_i}{\partial r}\frac{s^3t_i}{6}+\bar{A}_{22}h_i\frac{s^2t_i}{2}\right)\sigma_y\right]$$

$$\hat{P}_{3i}=\left[\left(\bar{A}_{11}\frac{\partial h_i}{\partial r}\frac{st_i}{2}+\bar{A}_{12}\frac{h_it_i}{2}\right)A_{\sigma1}+\left(\bar{A}_{21}\frac{\partial h_i}{\partial r}\frac{st_i}{2}+\bar{A}_{22}\frac{h_it_i}{2}\right)A_{\sigma3}+\frac{h_i}{x}\frac{st_i}{2}A_{\sigma5}\right]$$

$$\hat{Q}_{3i}=\left[\left(\bar{A}_{11}\frac{\partial h_i}{\partial r}\frac{st_i}{2}+\bar{A}_{12}\frac{h_it_i}{2}\right)A_{\sigma2}+\left(\bar{A}_{21}\frac{\partial h_i}{\partial r}\frac{st_i}{2}+\bar{A}_{22}\frac{h_it_i}{2}\right)A_{\sigma4}\right]$$

$$\tilde{P}_{3i}=\left[\left(\bar{A}_{11}\frac{\partial h_i}{\partial r}\frac{s^3t_i}{6}+\bar{A}_{12}h_i\frac{s^2t_i}{2}\right)A_{\sigma1}+\left(\bar{A}_{21}\frac{\partial h_i}{\partial r}\frac{s^3t_i}{6}+\bar{A}_{22}h_i\frac{s^2t_i}{2}\right)A_{\sigma3}+\frac{h_i}{x}\frac{s^3t_i}{6}A_{\sigma5}\right]$$

$$\tilde{Q}_{3i}=\left[\left(\bar{A}_{11}\frac{\partial h_i}{\partial r}\frac{s^3t_i}{6}+\bar{A}_{12}h_i\frac{s^2t_i}{2}\right)A_{\sigma2}+\left(\bar{A}_{21}\frac{\partial h_i}{\partial r}\frac{s^3t_i}{6}+\bar{A}_{22}h_i\frac{s^2t_i}{2}\right)A_{\sigma4}\right]$$

$$\begin{Bmatrix}A_{\sigma1}\\ A_{\sigma2}\\ A_{\sigma3}\\ A_{\sigma4}\\ A_{\sigma5}\end{Bmatrix}=\begin{Bmatrix}u_{,x}\sigma_x+u_{,y}\tau_{xy}\\ v_{,x}\sigma_x+v_{,y}\tau_{xy}\\ u_{,y}\sigma_y+u_{,x}\tau_{xy}\\ v_{,y}\sigma_y+v_{,x}\tau_{xy}\\ \frac{u}{x}\sigma_z\end{Bmatrix}$$

Appendix C

The incremental-iterative procedure, which is performed on the jth iteration of the ith incremental step, is according to the following steps:

1- Compute $\delta\lambda_1^i$: $\delta\lambda_1^i = \pm\delta\lambda_1^1 \left(\left| \frac{\delta u_{p1}^1 \cdot \delta u_{p1}^1}{\delta u_{p1}^{i-1} \cdot \delta u_{p1}^i} \right| \right)^{\frac{1}{2}}$

2- Compute the global tangent stiffness matrix K_j^i

3- Compute δu_{pj}^i : $\delta u_{pj}^i = \left(K_{j-1}^i \right)^{-1} p$

4- Compute δu_{rj}^i : $\delta u_{rj}^i = \left(K_{j-1}^i \right)^{-1} r_{j-1}^i$

5- Compute $\delta\lambda_j^i$: $\delta\lambda_j^i = \begin{cases} \dfrac{c}{\delta\lambda_1^i \, \delta u_{p1}^{i-1} \cdot \delta u_{p1}^i} & for \quad j = 1 \\ -\dfrac{\delta u_{p1}^{i-1} \cdot \delta u_{rj}^i}{\delta u_{p1}^{i-1} \cdot \delta u_{pj}^i} & for \quad j \geq 2 \end{cases}$ $\qquad c = \left(\delta\lambda_1^1 \right)^2 \left(\delta u_{p1}^1 \cdot \delta u_{p1}^1 \right)$

6- Update total load factor: $\lambda^i = \lambda^i + \delta\lambda_j^i$

7- Update external load vector: $\bar{p}^i = \bar{p}^i + \delta\lambda_j^i p$

8- Update total displacement vector: $u^i = u^i + \delta\lambda_j^i \delta u_{pj}^i + \delta u_{rj}^i$

9- Calculate the internal load $q\left(u^i\right)$

10- Compute unbalance load vector: $r_j^i = \bar{p}^i - q\left(u^i\right)$

11- The procedure continues from step 2 until the convergence criterion is achieved

References

[1] Librescu L., Refined geometrically nonlinear theories of anisotropic laminated shells, *Quarterly of Applied Mathematics*, 45(1), 1987, pp. 1-27.

[2] Dennis ST, Palazotte AN., Large displacement and rotational formulation for laminated shells including parabolic transverse shear, *International Journal of Non-Linear Mechanics*, 25(1), 1990, pp. 67-85.

[3] Alwar RS, Narasimhan MC., Axisymmetric non-linear analysis of laminates orthotropic annular spherical shells, *International Journal of Non-Linear Mechanics*, 27(4), 1992, pp. 611-622.

[4] Birman V., Axisymmetric bending of generally laminated cylindrical shells, *Journal of Applied Mechanics*, 60(1), 1993, pp. 157-162.

[5] Chandrashekhara K, Kumar BS., Static analysis of a thick laminated circular cylindrical shell subjected to axisymmetric load, *Composite Structures*, 23(1), 1993, pp. 1-9.

[6] Liu JH, Surana KS., Piecewise hierarchical p-version axisymmetric shell element for geometrically nonlinear behavior of laminated composites, *Computers & Structures*, 55(1), 1995, pp. 67-84.

[7] Ziyaeifar M, Elwi AE., Degenerated plate-shell elements with refined transverse shear strains, *Computers & Structures*, 60(6), 1996, pp. 428-460.

[8] Argyris J, Tenek L, Olofsson L., TRIC: a simple but sophisticated 3-node triangular element based on 6 rigid-body and 12 straining modes for fast computational simulations of arbitrary isotropic and laminated composite shells, *Computer Methods in Applied Mechanics and Engineering*, 145(1-2), 1997, pp. 11-85.

[9] Argyris J, Tenek L, Papadrakakis M, Apostolopoulou C., Postbuckling performance of the TRIC natural mode triangular element for isotropic and laminated composite shells, *Computer Methods in Applied Mechanics and Engineering*, 166(3-4), 1998, pp. 211-231.

[10] Pinto Correia IF, Barbosa JI, Mota Soares CM, Mota Soares CA., A finite element semi-analytical model for laminated axisymmetric shells: statics, dynamics and buckling, *Computers & Structures*, 76(1-3), 2000, pp. 299-317.

[11] Dumir PC, Joshi S, Dube GP., Geometrically nonlinear axisymmetric analysis of thick laminated annular plate using FSDT, *Composites Part B: Engineering*, 32(1), 2001, pp. 1-10.

[12] Pinto Correia IF, Mota Soares CM, Mota Soares CA, Herskovits J., Analysis of laminated conical shell structures using higher order models, *Composite Structures*, 62(3-4), 2003, pp. 383-390.

[13] Santos H, Mota Soares CM, Mota Soares CA, Reddy J.N., A semi-analytical finite element model for the analysis of laminated 3D axisymmetric shells: bending, free vibration and buckling, *Composite Structures*, 71(3-4), 2005, pp. 273-281.

[14] Wu CP, Pu YF, Tsai YH., Asymptotic solutions of axisymmetric laminated conical shells, *Thin-Walled Structures*, 43(10), 2005, pp. 1589-1614.

[15] Smith TA., Analysis of axisymmetric shell structures under axisymmetric loading by the flexibility method, *Journal of Sound and Vibration*, 318(3), 2008, pp. 428-460.

[16] Reddy JN., Refined nonlinear theory of plates with transverse shear deformation, *International Journal of Solids and Structures*, 20(9-10), 1984, pp. 881-896.

[17] Reddy JN., An evaluation of equivalent-single-layer and layerwise theories of composite laminates, *Copmosite Structures*, 25(1-4), 1993, pp. 21-35.

[18] Mantari JL, Oktem AS, Guedes Soares C., Static and dynamic analysis of laminated composite and sandwich plates and shells by using a new higher-order shear deformation theory, *Composite Structures*, 94(1), 2011, pp. 37-49.

[19] Han SC, Tabiei A, Park WT., Geometrically nonlinear analysis of laminated composite thin shells using a modified first-order shear deformable element-based Lagrangian shell element, *Composite Structures*, 82(3), 2008, pp. 465-474.

[20] Reddy JN, Liu CE., A higher-order shear deformation theory of laminated elastic shells, *International Journal of Engineering Science*, 23(3), 1985, pp. 319-330.

[21] Noor AK, ASCE M, Peters JM., Analysis of laminated anisotropic shells of revolution, *Journal of Engineering Mechanics*, 113(1), 1987, pp. 49-65.

[22] Sheinman I, Shaw D, Simitses GJ., Nonlinear analysis of axially-loaded laminated cylindrical shells, *Computers & Structures*, 16(1-4), 1983, pp. 131-137.

[23] Patel BP, Singh S, Nath Y., Postbuckling characteristics of angle-ply laminated truncated circular conical shells, *Communications in Nonlinear Science Numerical Simulation*, 13(7), 2008, pp. 1411-1430.

[24] Singh S, Patel BP, Nath Y., Postbuckling of laminated shells of revolution with meridional curvature under thermal and mechanical loads, *International Journal of Structural Stability and Dynamics*, 9(1), 2009, pp. 107-126.

[25] Cagdas IU., Stability analysis of cross-ply laminated shells of revolution using a curved axisymmetric shell finite element, *Thin-Walled Structures*, 49(6), 2011, pp. 732-742.

[26] Wu CP, Chi YW., Three-dimensional nonlinear analysis of laminated cylindrical shells under cylindrical bending, *European Journal of Mechanics- A/Solids.* 24(5), 2005, pp. 837-856.

[27] Bhaskar K, Varadan TK., A higher-order theory for bending analysis of laminated shells of revolution, *Computers & Structures*, 40(4), 1991, pp. 815-819.

[28] Bhimaraddi A, Carr AJ, Moss PJ., A shear deformable finite element for the analysis of general shells of revolution, *Computers & Structures*, 31(3), 1989, pp. 299-308.

[29] Chang TY, Sawamiphakdi K., Large deformation analysis of laminated shells by finite element method, *Computers & Structures*, 13, 1981, pp. 331-340.

[30] Rezaiee-Pajand M, Arabi E., A curved triangular element for nonlinear analysis of laminated shells, *Composite Structures*, 153, 2016, pp. 538-548.

[31] Xu CS., Buckling and post-buckling of symmetrically laminated moderately-thick spherical caps, *International Journal of Solids and Structures*, 28(9), 1991, pp. 1171-1184.

[32] Alankaya V, Oktem AS., Static analysis of laminated and sandwich composite doubly-curved shallow shells, *Steel and Composite Structures*, 20(5), 2016, pp. 1043-1066.

[33] Sofiyev AH, Kuruoglu N., Buckling of non-homogeneous orthotropic conical shells subjected to combined load, *Steel and Composite Structures*, 19(1), 2015, pp. 1-19.

[34] Rezaiee-Pajand M, Arabi E, Masoodi Amir R., A triangular shell element for geometrically nonlinear analysis, *Acta Mechanica*, 229(1), 2018, pp. 323-342.

[35] Santos H, Mota Soarez CM, Mota Soarez CA, Reddy JN., A semi-analytical finite element model for the analysis of cylindrical shells made of functionally graded materials, *Composite Structures*, 91(4), 2009, pp. 427-432.

[36] Bich DH, Dung DV, Hoa LK., Nonlinear static and dynamic buckling analysis of functionally graded shallow spherical shells including temperature effects, *Composite Structures*, 94(9), 2012, pp. 2952-2960.

[37] Bich DH, Tung HV., Non-linear axisymmetric response of functionally graded shallow spherical shells under uniform external pressure including temperature effects, *International Journal of Non-linear Mechanics*, 46(9), 2011, pp. 1195-1204

[38] Zozulya VV. Zhang CH., A high order theory for functionally graded axisymmetric cylindrical shells, *International Journal of Mechanical Sciences*, 60(1), 2012, pp. 12-22.

[39] Viola E, Rossetti L, Fantuzzi N, Tornabene F., Static analysis of functionally graded conical shells and panels using the generalized unconstrained third order theory coupled with the stress recovery, *Composite Structures*, 112, 2014, pp. 44-65.

[40] Arciniega RA, Reddy JN., Large deformation analysis of functionally graded shells, *International Journal of Solids and Structures*, 44(6), 2007, pp. 2036-2052.

[41] Kar VR, Panda SK., Nonlinear flexural vibration of shear deformable functionally graded spherical shell panel, *Steel and Composite Structures*, 18(3), 2015, pp. 693-709.

[42] Wu CP, Liu YC., A state space meshless method for the 3D analysis of FGM axisymmetric circular plates, *Steel and Composite Structures*, 22(1), 2016, pp. 161-182.

[43] Surana KS., Geometrically nonlinear formulation for the axisymmetric shell elements, *International Journal for Numerical Methods in Engineering*, 18(4), 1982, pp. 477-502.

[44] Leon SE, Paulino GH, Pereira A, Menezes IFM, Lages EN., A unified library of nonlinear solution schemes, *Applied Mechanics Reviews*, 64(4), 2011, pp. 1-26.